The Role of Electron Spin-Polarizability and Charge Dynamics in Protein Function

Pratik Vyas[1*#], Kakali Santra[1#], Naupada Preeyanka[1], Anu Gupta[1], Orit Weil-Ktorza[2], Qirong Zhu[1], Liam M. Longo[3,4], Jonas Fransson,[5] Norman Metanis,[2] and Ron Naaman[1*]

[1]Department of Chemical and Biological Physics, Weizmann Institute of Science, Rehovot, 76100, Israel.

[2]Institute of Chemistry, The Hebrew University of Jerusalem, Jerusalem 9190401, Israel

[3]Earth-Life Science Institute, Tokyo Institute of Technology, Tokyo 152-8550, Japan

[4]Blue Marble Space Institute of Science, Seattle, Washington 98104, USA

[5]Department of Physics and Astronomy, Uppsala University, Uppsala 752 36, Sweden

[#]Equal contribution

*Corresponding authors:

Ron Naaman: ron.naaman@weizmann.ac.il;

Pratik Vyas: pratik.vyas@weizmann.ac.il; prateekvyas07@gmail.com

Abstract:

We investigated the association of two model primordial polypeptides, each bearing an ancient and ubiquitous phosphate-binding motif, with DNA. The association rate and the amount of bound DNA relates to the electron spin-dependent polarizability of the binding protein. Contributions to protein polarizability are also made by residues that are far from the spin injection site. The spin-dependence is associated with the chirality of the proteins and is a consequence of chiral-induced spin selectivity (CISS). Since the polypeptides studied are hypothesized to be among the initial stand-alone 'seed' fragments from which contemporary protein domains evolved, the results suggest the importance of spin-dependent polarizability early in protein evolution. As the spin effect is a direct consequence of biopolymer homochirality, it was likely significant from even the earliest stages of biological evolution. We provide model calculations clarifying the underlying reasons for spin selectivity and estimating its impact on protein function.

Introduction:

The recognition between proteins and their binding partners is influenced by electrostatic interactions. These interactions stem from charged groups located at or near the binding site that can modulate the diffusion-limited association rate.[1–3] Accordingly, theoretical analyses of protein interactions regularly account for the static charge distributions of protein surfaces.[4] However, it is known that in addition to static charges, the interaction of the protein with any substrate also results in a dynamic charge redistribution in the protein. This redistribution is related to electrical polarizability – the property of a material, including biomolecules, to become polarized in the presence of an electric field. This polarizability stems from both the displacement of charged groups due to the electric field and the redistribution of electronic densities relative to the nuclei. It is important to appreciate that the binding of a protein/enzyme to its cognate ligand/substrate is analogous to applying an electric field to the protein.[5] Indeed, the significance of polarizability in protein structure and activity is increasingly recognized and recent calculations have begun to take it into account.[6–9]

Given the inherent polarizability of proteins, we have recently demonstrated that allosteric effects can occur through charge redistribution in the protein and this charge redistribution depends on the spin of the electrons that are redistributed.[10,11] This electrostatic effect is non-localized, controlled by the withdrawal of charge from sites remote from the active site and redistributed to sites throughout the protein structure. This form of allostery was dubbed charge-reorganization allostery (CRA).[10,11] For the systems studied, it was observed that CRA depends on the spins of the electrons being reorganized. This was attributed to the chiral-induced spin-selectivity (CISS) effect, which refers to the experimental observation that the motion of electrons through or within chiral molecules (and materials) depends on their spin state. Which spin is preferred depends on the handedness of the molecule and on the direction of motion of the electrons.[12] While for one handedness the preferred spin will be always pointing parallel to the velocity of the electrons, for the opposite handedness it will always point antiparallel to the velocity. A consequence of this effect is that the movement of electrons in a chiral molecule generates not only a charge-polarization (*i.e.*, a separation of positive and negative charges within the molecule), but also spin-polarization (*i.e.*, a preference for electrons with one specific spin, either "up" or "down") such that one spin has higher density at one electric pole and the other at the opposite pole.[13]

An important and unexplored question pertains to the significance of electron spin selectivity throughout the history of protein evolution: Can charge-based allostery and spin selectivity be detected in primitive binding events? And, if these phenomena are detected, to what extent could they have promoted or constrained ligand binding by the earliest protein forms?

Given the structural and functional complexity of modern proteins, the primordial states from which these intricate enzymes evolved are difficult to discern. Recent evidence suggests, however, that many contemporary proteins condensed around relatively short 'seeding' peptides with simple secondary structures.[14–22] These evolutionary nuclei – despite billions of years of evolution – have remained largely unchanged on account of their profound functional importance. A prime example of such a peptide is the phosphate-binding loop (P-loop) of the ancient and ubiquitous enzyme family P-Loop NTPases.[23–26] Originally, identified in ATP synthases and ATPases, the P-loop is rich in glycine and binds phosphate-containing ligands via the N-terminus of an α-helix, a primitive binding mode.[22] Characterized by the conserved Walker A motif, GxxGxGK(T/S), this functional element binds phosphorylated cofactors such as ATP [27] and DNA [28,29] as well as catalyzes phosphoryl-transfer reactions.[17,27,30,31] Structurally, the P-loop is flanked by a β-strand and an α-helix to form a β-(P-loop)-α motif. This structural β-(P-loop)-α motif is common to various enzyme families and is generally considered to have sparked the emergence of several enzyme families independently.[20,21,32,33]

We have previously described short βα polypeptides (~50 residues) bearing a single, ancestrally inferred β-(P-loop)-α motif.[17,29] Despite their simplicity and the lack of auxiliary catalytic residues that are found in contemporary P-loop NTPases, these polypeptides, dubbed P-loop prototypes, demonstrate binding to various phosphorylated-ligands such as ATP, inorganic polyphosphates, and DNA. Moreover, these polypeptides were able to mediate elementary yet elaborate biochemical reactions such as DNA unwinding and phosphoryl-transfer.[17,29] It is noteworthy that binding to phosphate ligands, including nucleic acids, nucleotides, and nucleotide cofactors, is a fundamental and ancient function.[17–22,29] Therefore, the functions performed by P-loop prototypes not only relate to modern P-loop enzymes, but also hold evolutionary significance and relevance in the context of a primordial world. P-loop prototypes, thus, serve as credible and tangible representations of early 'founder enzymes' and simultaneously function as evolutionary missing links, bridging primitive enzymes and their present-day counterparts. Given the above, P-

loop prototypes are an ideal experimental system to explore the historical and contemporary significance of electron-spin selectivity.

Two P-loop prototypes were selected to explore the role of charge and electron spin polarization in the phosphate binding: N-αβα and N-βα (**Figures 1A and 1B**).[29] The N-αβα prototype was chosen because it shows good expression and purification yields, whereas the N-βα construct was chosen because it comprises just the β-(P-loop)-α motif.

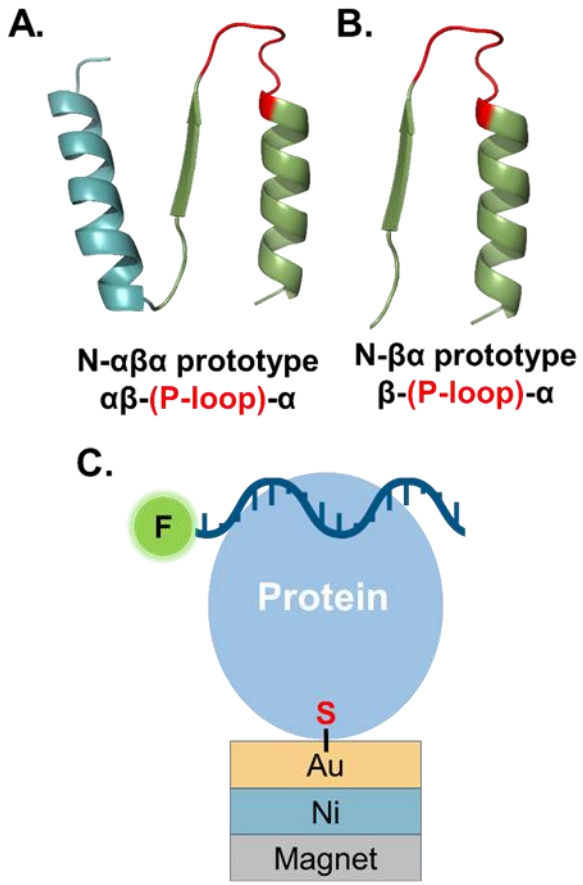

Figure 1: Representative P-loop prototypes and experimental setup. A. The N-αβα prototype comprises the ancestral β-(P-loop)-α motif and one additional α-helix at the N-terminus. **B.** The N-βα prototype comprises only of the ancestral β-(P-loop)-α motif. The structural models in panels A and B depict the ancestrally inferred β1 and α1 in green and the connecting P-loop in red. The additional α-helix in the N-αβα prototype is shown in cyan. The descriptor below each prototype indicates the strand topology and the order of secondary structural elements (from N- to C-terminus). The prototypes have a propensity to form dynamic oligomers in solution [17,28,29]; therefore, the monomeric models shown here are only schematic depictions. **C.** Schematic of the experimental setup. Proteins carrying a C-terminal cysteine with a free thiol (-SH) group are adsorbed onto a gold-coated, ferromagnetic nickel layer via an S-Au bond. The ferromagnetic substrates (FM-substrates) with the adsorbed proteins are then placed onto a permanent magnet. The entire assembly (magnet + FM-substrates) is transferred to a microscope and binding to fluorescent DNA is monitored. The experiments were carried out with both orientations of magnet (North and South) facing. Figure panel C was partly created using BioRender.com

To probe the dependence of DNA-binding on electron spin polarizability, P-loop prototypes were adsorbed onto ferromagnetic substates (FM-substrates) that serves as a source for spin polarized charge. To facilitate the adsorption, a cysteine (thiol) residue is incorporated into the prototypes at the C-terminal end. Amino acid sequences are provided in **Supplementary Table**

S2 and substrate preparation is described in the **Methods** section. The immobilization of the prototypes occurred via the formation of sulfur-gold bond between a cysteine residue and the gold monolayer on the FM-substrate (**Figure 1C**). The FM-substrates were then placed on a magnet with one polarity facing the substrate and held in place using adhesive tape. In parallel, a Petri dish containing fluorescent DNA in buffered solution was transferred to the stage of a wide-field microscope. The magnet assembly (*i.e.*, the magnet, substrates, and prototypes) was then inverted onto the Petri dish with fluorescent DNA and the time-dependent increase in fluorescence intensity was measured. The same process was repeated with the opposite polarity of magnet facing the substrate (see **Methods**). We will refer to magnet orientations as either UP (North magnet pole facing the FM-substrates) or DOWN (South magnet pole facing the substrates). The orientation of the ferromagnet defines the electron spin that can be injected into the substrate or ejected from the substrate.

Our working hypothesis is structured as follows: when a DNA molecule approaches the binding site of a protein, electrostatic interactions between the two induces a charge reorganization within the protein, *i.e.*, electrons are either accumulated at or repelled away from the binding site. The direction of the charge motion and its magnitude depends on the sign and amount of the charge on the DNA as well as on the inherent polarizability of the protein. The larger the polarizability of the protein, the more pronounced the charge reorganization induced by DNA at the binding site of the protein will be. It is known that the efficiency of electron injection into ferromagnet (onto which the proteins are adsorbed) depends on the spin states of the electrons and the magnetization direction of the substrate. Hence, if the charge reorganization within the protein is spin-dependent – meaning that only electrons with a specific spin are repelled away from the binding site, in accordance with the CISS effect – then for one direction of the magnet relative to the substrate, electrons will be able to be injected into the substrate; however, for the opposite magnetization, electrons will not be injected. Consequently, we anticipate that the polarizability of the protein, and hence its binding affinity to DNA, will vary with the magnetization direction of the substrate. This could lead to a magnetization-dependent and spin-dependent modulation of protein-DNA interactions.

Results

It was previously demonstrated that the N-αβα prototype showed preferential binding to fluorescently-labeled ssDNA that is rich in thymine and cytosine nucleotides[29] (K_D = 0.67±0.16 μM; hereafter referred as TC-ssDNA, **Supplementary Figure S1; Supplementary Tables S3** and **S4**). Therefore, we used the same DNA for testing the phosphate binding function of this construct. **Figure 2A** presents adsorption isotherms of TC-ssDNA binding to N-αβα prototype with the magnet pointing towards the molecules (UP) or away from them (DOWN). The resulting time-dependent increase in fluorescence intensity shows that the binding rate and the amplitude of the fluorescence increase (*i.e.*, the amount of prototype-bound DNA) is larger when the ferromagnet is aligned UP (**Figure 2A, Table 1**). To verify that the observed increase in fluorescence is not an artifact of the N-αβα prototype interacting with the fluorophore on the DNA, but rather a consequence of prototype-DNA binding, we measured the adsorption of nuclease-digested TC-ssDNA (which lacks intact DNA) to the N-αβα prototype-coated substrate. In this case, only a very small effect of the magnetic field is observed (**Supplementary Figure S2**). Next, we examined the binding of ssDNA that is rich in guanines and adenines (henceforth referred to as GA-ssDNA; **Figure 2B**) and has been previously demonstrated to bind weakly to P-loop prototypes[29] (K_D = 1.70±0.68 μM; **Supplementary Figure S1**; **Supplementary Table S3** and **S4**). In this case, when the magnet is pointing UP, the magnitude of GA-ssDNA binding is lower compared to TC-ssDNA and the adsorption (binding) profiles are similar for both magnetic field orientation (*i.e.*, no preference for UP or DOWN orientation, **Figure 2B**).

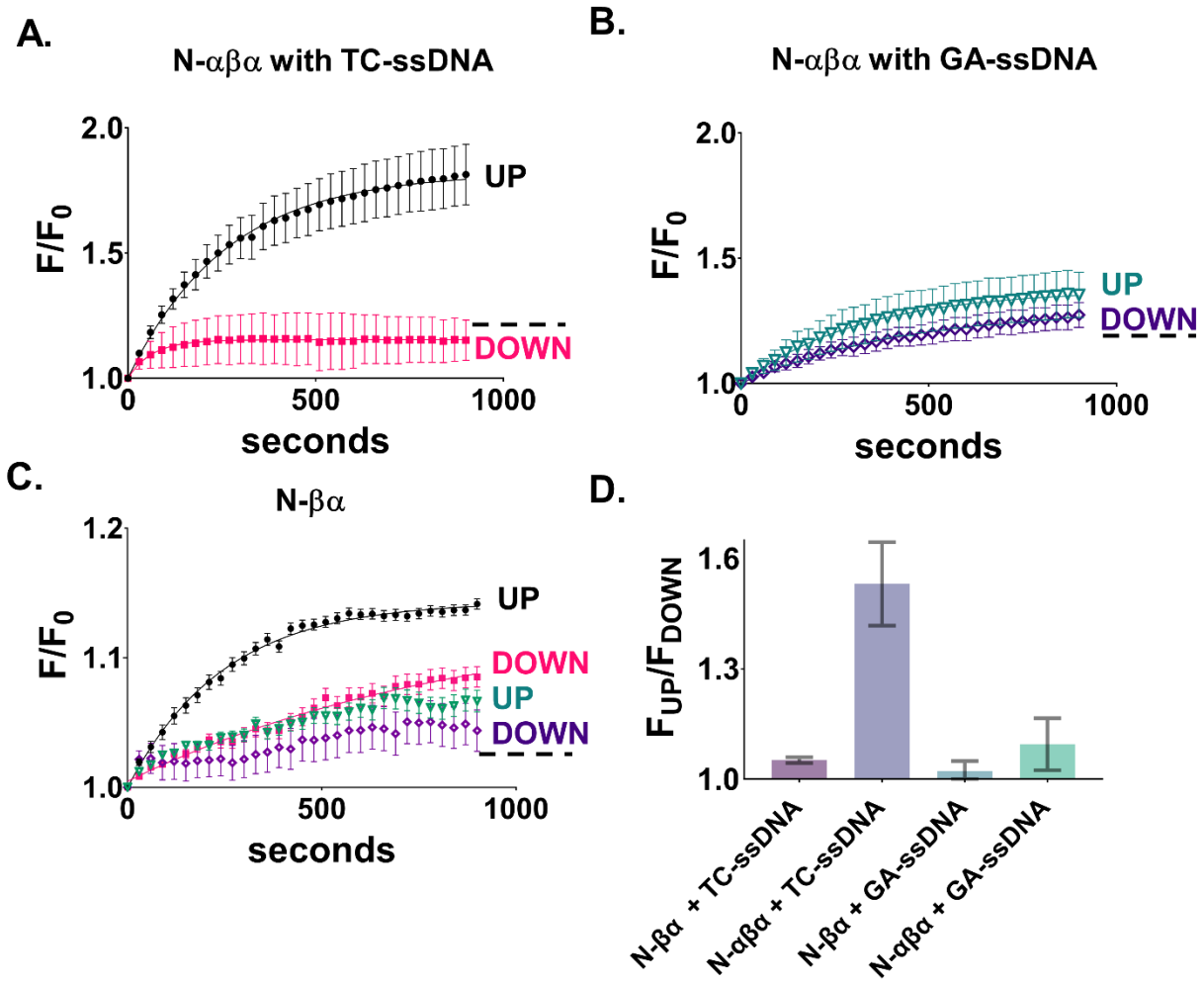

Figure 2: Spin selectivity of DNA binding to N-αβα and N-βα prototypes. Adsorption isotherms showing binding of **A.** TC-ssDNA to N-αβα prototype for UP (black trace) and DOWN (pink trace) orientations and **B.** GA-ssDNA to N-αβα prototype for UP (green trace) and DOWN (purple trace) orientations. **C.** Adsorption isotherms showing binding of N-βα prototype to TC-ssDNA for UP (black trace) and DOWN (pink trace) orientations and to GA-ssDNA for UP (green trace) and DOWN (purple trace) orientations. Fits to data in panels A, B, and C were from a standard one-phase association equation using GraphPad Prism and error bars represent standard deviation from three to four independent measurements. Dotted lines in A, B, and C depict background binding to the fluorescein dye (see also **Supplementary figure S2**) **D.** Relative fluorescence increases. The bar graph displays the relative difference in the endpoint-F/F_0 values corresponding to the binding of each prototype (N-αβα or N-βα) to each DNA sequence (TC-ssDNA or GA-ssDNA). Here, the endpoint fluorescence value of the magnet in the UP orientation was divided by the endpoint fluorescence value of the magnet in the DOWN orientation for the same DNA-protein pair to give relative ratios (F_{UP}/F_{DOWN}). Error bars represent the standard deviation of three independent replicates.

To investigate the role of secondary structure elements on the spin-selective behavior of the prototypes, we tested the binding of the N-βα prototype, which lacks the N-terminal α-helix (**Figure 1B**). The N-βα prototype demonstrated favored binding to TC-ssDNA with the magnet in the UP orientation compared to the DOWN orientation, as is the case of the N-αβα prototype. For the UP orientation, the amplitude of fluorescence increase for TC-ssDNA is greater than the disfavored GA-ssDNA. On the other hand, the binding of GA-ssDNA for both magnet orientations are comparable, indicating decreased spin-selectivity at this magnetic field strength (**Figure 2C**). Thus, similar to N-αβα, the N-βα prototype also shows spin preference. However, the magnetic field effect is notably smaller for the N-βα prototype than it is for the N-αβα prototype, like owing to the overall weaker binding of this construct (**Figure 2D**).

Next, we determined the relationship between the preferred magnetic orientation and the handedness of the P-loop prototypes. As described earlier, the prototypes have a C-terminal cysteine residue that serves as a 'linker' between the protein and the magnetized FM-substrate – the site for electron injection. N-αβα prototypes that have opposing handedness of the terminal cysteine residue were chemically synthesized. One peptide (N-αβα_LcysEnd) consists of all amino acids in their *L*-form whereas the other peptide (N-αβα_DcysEnd) is identical except for the terminal cysteine, which is in the *D*-form (**Supplementary Table S2**). The N-αβα_LcysEnd peptide exhibited spin-selective behavior and a preference for the UP orientation, similar to the *E. coli*-expressed N-αβα prototype, which is presumed to contain only *L*-isomers (**Figure 3A**). However, for the N-αβα_DcysEnd peptide, no binding was observed in the UP orientation whereas stronger binding was observed in the DOWN orientation (**Figure 3B**). Overall, these results indicate spin-selective binding of P-loop prototypes to DNA.

The observed spin selectivity can, in principle, be a result of the spin-dependent charge polarizability within the proteins or due to the spin-dependent interaction between the DNA and the protein. The question of which mechanism is the dominant one can be resolved by studying the spin-dependent association with proteins that are composed exclusively *L*- or *D*-amino acids, thus inverting the entire handedness of the protein construct (including their DNA-binding sites) and assuming that the binding mode is largely unchanged. To this end, we characterized two model peptides derived from an ancestor sequence reconstruction and amino acid deconstruction[34] of the

ancient and ubiquitous helix-hairpin-helix (HhH) family[35] and consisting entirely of either *L*- or *D*-amino acids[36] (see **Supplementary Table S2** for peptide sequences). Despite total chiral inversion (all amino acids changed from *L*- to *D*-form), these peptides have been shown to retain their ability to form coacervates with *D*-RNA.[36] Molecular dynamics simulations suggest that the primary interaction with RNA is mediated by positively-charged side chains,[37] a fact consistent with the observed functional robustness to chiral inversion. **Figures 3C** and **3D** show binding of dsDNA by the HhH peptides *L*-Precursor and *D*-Precursor to a fluorescent 12-bp dsDNA using the same experimental setup described above (**Figure 1C**). **Figure 3C** shows that the *L*-Precursor construct binds dsDNA faster when the substrate is magnetized DOWN than when it is magnetized UP. In contrast, the *D*-Precursor construct binds faster with the opposite (UP) orientation of the substrate. The rates of binding for the *L*- and *D*-peptides are similar for the favored spins (**Table 1**), suggesting that while spins influence the polarizability of the peptides, resulting in inverted spin preferences for the two enantiomers, the actual rate of binding, once polarizability is maximized, is the same for the two enantiomers. Consequently, the interaction between the DNA and the peptide is not spin dependent, and the observed effect is instead the result of spin-dependent charge polarizability within the protein. This finding supports the conclusion that the interaction is predominantly electrostatic without significant selectivity to the chiral structure.

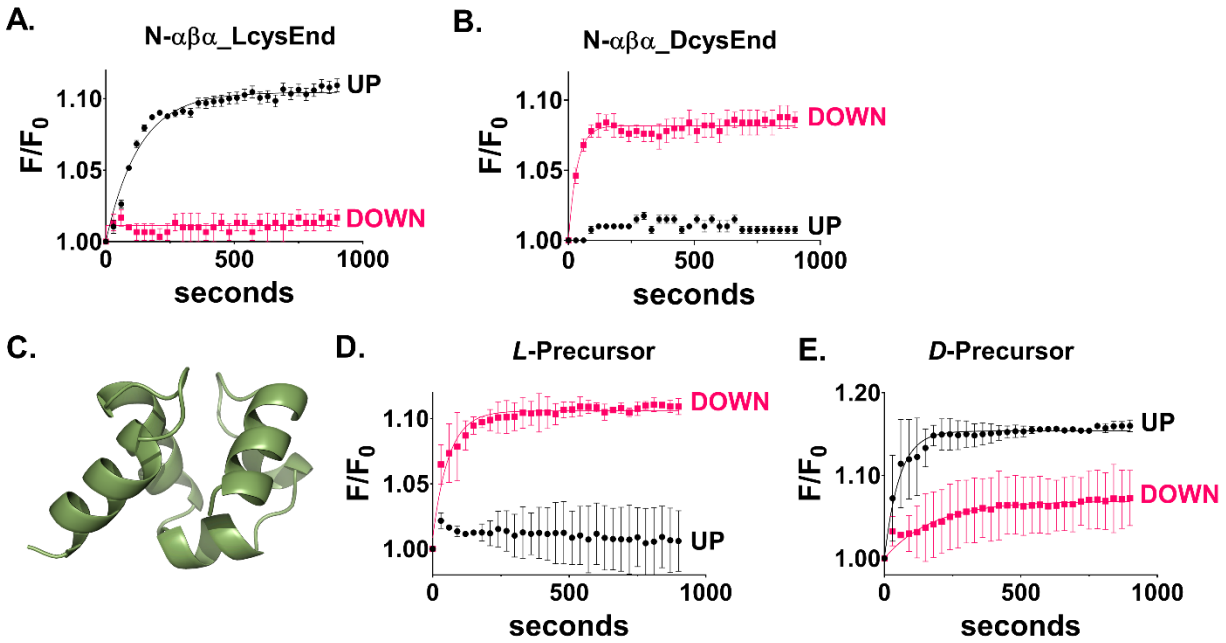

Figure 3: Handedness effect on the magnetism-dependent association. The influence of handedness of synthetic P-loop prototypes and HhH polypeptides on binding to TC-ssDNA or 12-

bp dsDNA, respectively, for both magnet orientations. **A.** Adsorption isotherms of TC-ssDNA binding to N-αβα anchored to a ferromagnetic surface via *L*-cysteine (N-αβα_LcysEnd). **B.** Same as A but with N-αβα anchored via *D*-cysteine (N-αβα_DcysEnd). **C.** AlphaFold2 model of the $(HhH)_2$-fold, which is recapitulated upon dimerization of two HhH peptides[37] **D.** Adsorption isotherms of 12-bp dsDNA binding to the Precursor-Arg peptide, which is comprised of a single HhH motif, and for which with all amino acids are in the *L*-form (*L*-Precursor) **E.** Same as C but for with all amino acids in the *D*-form (*D*-Precursor). Error bars represent standard deviation from three to four independent measurements. We note that the amplitude of the fluorescence increases for the N-αβα_LcysEnd construct ($F/F_0 \sim 1.1$) is slightly less than its biologically-produced counterpart ($F/F_0 \sim 1.8$, Figure 2A). This difference is likely due to the inherent oligomeric heterogeneity of the N-αβα prototype across various batches of purification.[29] Nonetheless, the relative preference for the UP vs DOWN orientation remains unchanged.

Table 1: Apparent rate constants of DNA binding to adsorbed P-loop prototypes and HhH polypeptides.

	TC-ssDNA		**GA-ssDNA**	
	UP	**DOWN**	**UP**	**DOWN**
N-αβα	4 (0.1) E-03 $R^2 = 0.99$	--	3 (0.8) E-03 $R^2 = 0.98$	--
N-βα	4 (0.2) E-03 $R^2 = 0.99$	1 (0.2) E-03 $R^2 = 0.98$	3 (0.1) E-03 $R^2 = 0.95$	0.7 (0.4) E-03 $R^2 = 0.88$
N-αβα_LcysEnd	6 (2) E-03 $R^2 = 0.97$	--		
N-αβα_DcysEnd	--	8 (4) E-03 $R^2 = 0.98$		
	12-bp dsDNA			
	UP	**DOWN**		
***L*-Precursor**	1.9 (0.1) E-02 $R^2 = 0.82$	--		
***D*-Precursor**	--	1.8 (0.5) E-02 $R^2 = 0.76$		

Rate constants were determined by fitting the data to a standard one-phase association equation in the GraphPad Prism software. Numbers in parenthesis indicates standard deviation from three to four independent measurements. Amino acid sequences are provided in **Supplementary Table S2**. Nucleotide sequences of TC-ssDNA, GA-ssDNA and 12-bp dsDNA are provided in **Supplementary Table S3**.

Lastly, as an independent verification of the results obtained using fluorescence microscopy, we performed contact potential difference (CPD) studies with a Kelvin probe [38] (**Figure 4**). These measurements allowed us to confirm the role of spin transport in the protein-DNA interaction. The Kelvin probe setup (*Delta Phi Besocke, Jülich, Germany*) was located inside

a Faraday cage at ambient conditions. The setup includes a metallic probe electrode (gold grid) placed near the surface of the sample to form a capacitor (**Figure 4A**). The distance between the probe electrode and the surface of the sample is periodically varied to create a frequency dependent capacitance. As a result of the CPD, an AC voltage is generated across the gap, and it is proportional to the difference in the work-function between the sample and the probe electrode. A DC voltage is applied to nullify the AC voltage. A more negative value indicates that the adsorbate reduced the work-function more significantly.

Here, the N-αβα_LcysEnd construct was adsorbed onto FM-substrates, as with the previous experiments. Substrates were then placed onto a permanent magnet with the North polarity facing the substrate (UP) or away from the substrates (DOWN). A drop of TC-ssDNA solution (or buffer alone as a control) was the placed onto the adsorbed proteins and incubated for 30 min at room temperature. CPD values were then measured using the setup depicted in **Figure 4A** (see **Methods** for details on the experimental setup and substrate preparation). The results indicate that when the magnet North pole is pointing UP, the work-function becomes less negative (higher work-function) than for adsorption occurring with the magnet pointing DOWN (**Figure 4B**). This indicates more adsorption of DNA onto the protein-coated surface for the UP configuration. Hence, the Kelvin probe microscopy experiments provide an independent verification of the results obtained from fluorescence microscopy experiments.

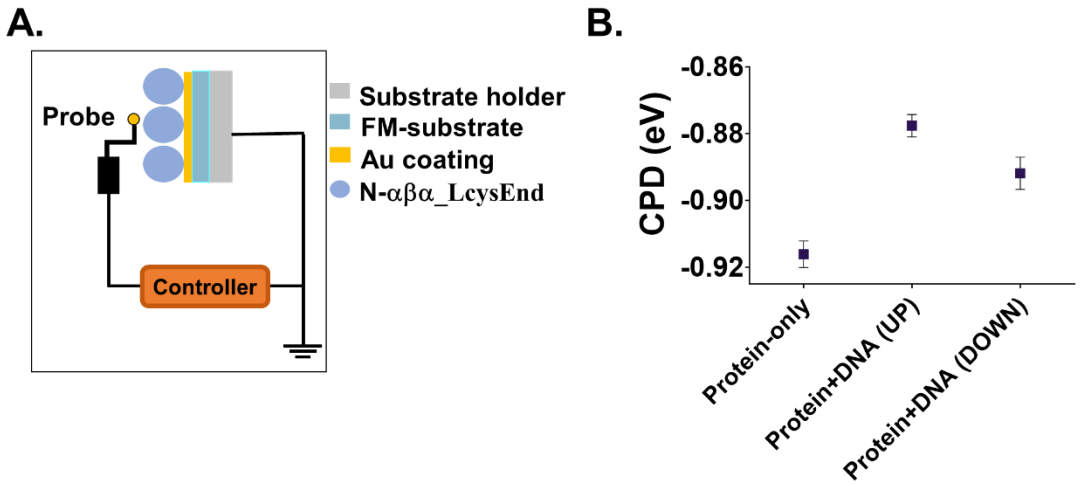

Figure 4. **A.** Schematic of the Kelvin probe setup. **B.** The measured CPD values for the N-αβα_LcysEnd construct. CPD (eV) values were measured for 'Protein-only' (adsorbed protein without incubation with DNA), 'Protein+DNA (UP)' (adsorbed protein incubated with DNA with magnet facing the substrates) and 'Protein+DNA (DOWN)' (adsorbed protein incubated with

DNA with magnet facing away from substrates). Error bars represent standard deviation from two independent experiments.

Discussion

The results indicate that P-loop prototypes and deconstructed HhH peptides demonstrate chiral-induced spin-selective behavior, which in turn governs phosphate binding. The extent of the spin-selective effect depends on the strength of binding. In the case of relatively strong binding, such as of the P-loop prototypes to the TC-rich sequence or of the HhH peptides to dsDNA, the amount of charge that is reorganized is large, and hence charge has to be spread all over the system. However, for GA-rich DNA where the binding to the P-loop prototype is weak, only a small amount of charge reorganization occurs and, consequently, the charge reorganization is short range and does not result in a significant charge exchange with the substrate (**Figure 2A, 2B**). The magnitude of the spin-selective charge redistribution depends also on the polarizability of the system. This is demonstrated by the removal of the N-terminal α-helix, distant from the C-terminal electron injection site, resulting in a diminished magnitude of spin-selective behavior. Although the exact structure of the P-loop oligomer is unknown, this result suggests that structural elements distinct from the primary binding-site residues can affect reactivity due to their contribution to the polarizability of the protein. In other words, the α-helix serves as a reservoir of charge that participates in charge reorganization within the protein upon binding to DNA, even though it is not likely a primary interaction site (**Figure 2C, 2D**).

We show that protein handedness influences the spin behavior of not only P-loop prototypes [17,29], but also regulates function of primordial peptides from another ancient protein-motif – the nucleic acid-binding HhH motif (**Figure 3**).[34,35] Considering the fundamental and 'simple' nature of this phenomenon, we propose that allosteric interactions based on charge reorganization and chiral-induced electron-spin selectivity represents a plausible contributor to biomolecular recognition early in protein evolution. Furthermore, P-loop prototypes and HhH peptides leverage functional motifs that have persisted into the preset day. As such, it is reasonable to assume that electron spin selectivity and the resultant polarizability underlie functions mediated by contemporary proteins and enzymes as well. Lastly, as described below, the importance of spin selectivity is rationalized and supported by model calculations (**Figures 5 and 6**).

The results indicate the strong dependence of the association rate and the extent of protein-DNA binding on the direction of the substrate's magnetic field. The dependence is very pronounced, to the extent that in some cases, the unfavorable magnetic field direction blocks the association between the DNA and the proteins (see **Figure 1A, 3A and 3D**). When the proteins are made from *D*-amino acids (**Figure 3E**) or the binding to the substrate is through *D*-cysteine (**Figure 3B**), the preferred direction of the magnetic field switches. **Figure 5** schematically presents the mechanism of this effect, which is based on the special properties of chiral systems – the spin-selective transport of electrons via the CISS effect.

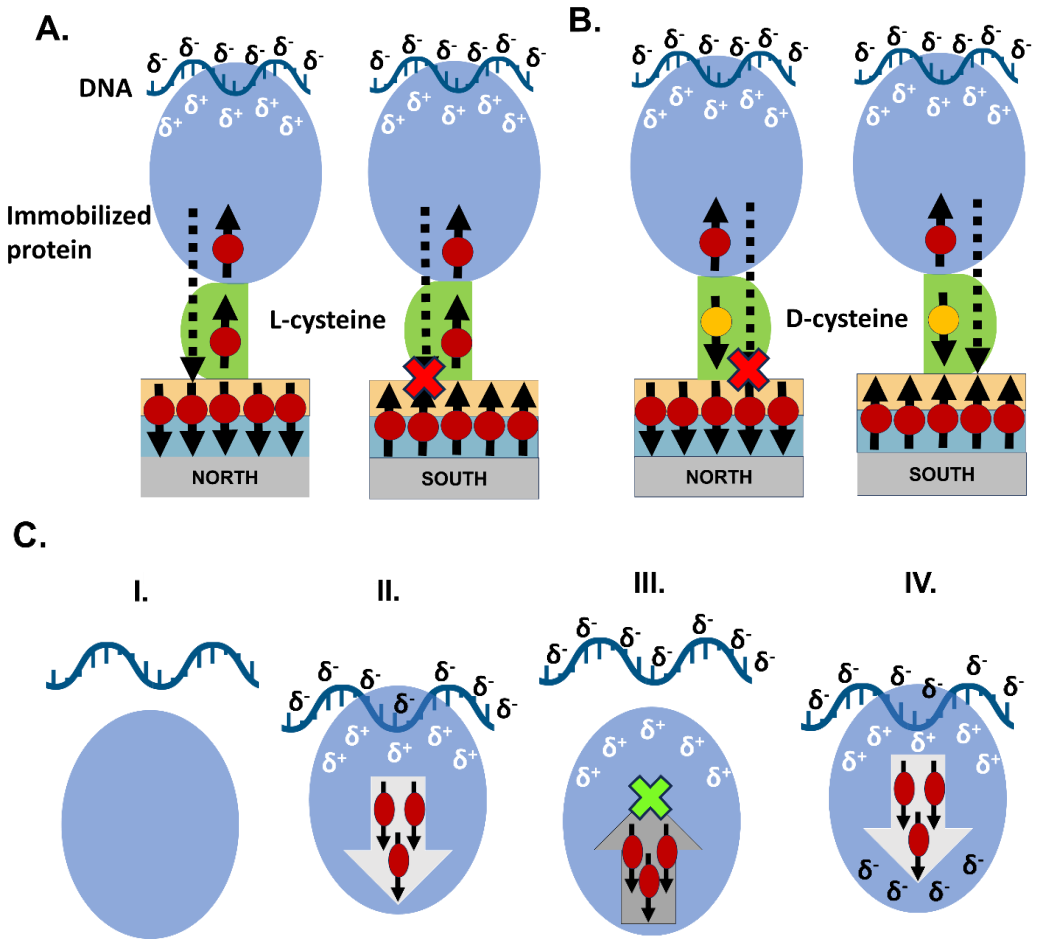

Figure 5: A. Schematic representation of the mechanism of the effect of spin on the protein-DNA interaction. When the spin on the ferromagnet is pointing opposite to the momentary spin of the charge at the interface of the adsorbed proteins (spins shown as black arrows and electrons are shown as red ball), charge flows more efficiently between the protein and FM-substrate. This scenario manifests when the North magnet is facing the FM-substrate. When the South magnet is

facing the FM-substrate, the spins on the protein and the substrate are pointing the same direction resulting in inefficient electron-flow. **B.** Effect of the *D*-cysteine linker on protein-DNA interaction. The terminal *D*-cysteine linker, shown in green, which has the opposing chirality to the rest of the protein, flips the direction of spins transmitted through the protein. Consequently, the opposite magnet polarity is required to achieve electron-flow, relative to the schematic in A. **C.** Model describing the role of electrons spin-related polarizability in protein function. Reaction scheme describes the dynamic interaction of a protein molecule with a DNA molecule to form transient (Protein-DNA)' complex (charge-reorganization step) and the final energetically favored (Protein-DNA) configuration (binding step). Figure 5 was partly created using BioRender.com.

When the DNA approaches the protein adsorbed on the ferromagnet, it induces polarization of the charge in the protein. Here we refer not to the charge localized on specific functional groups, but rather to charge that can be delocalized. This polarization is related to the high frequency polarizability of the protein, or in other terms, to the protein's high frequency dielectric constant. Since the DNA is negatively charged, when it approaches the protein electrons are repelled from the binding site (**Figures 5A, B**). Because of the chirality of the protein, the charge rearrangement depends on the electrons' spin.[13] Namely, electrons with one spin orientation move more efficiently through the protein. If the substrate is magnetized so that the electrons with the preferred spin can be injected into it, then the electrons withdrawn from the binding site can move into the ferromagnet, thereby the effective polarizability of the protein increases. In the specific case of *L*-proteins, this means that since the preferred spin for electrons motion is the spin antiparallel to the electrons' velocity, the ferromagnet should be aligned with its North pole pointing towards the protein (namely its majority spin is aligned away from the protein) and therefore the electrons from the protein can be injected into the minority states of the ferromagnet (**Figure 5A**).

The spin dependency of the association is surprising, and the question is if it serves any function in biological systems. In what follows we will present a possible explanation for the importance of the spin. It is well accepted that the "docking" of substrates/ligands on enzymes/proteins is not an abrupt single-step event but a rather a dynamic process, influenced by the conformational dynamics of the participating biomolecules, involving multiple 'binding-unbinding' events, till the minimum-energy configuration is achieved.[39–43] Upon the first encounter of the DNA and the protein, electrostatic interactions induces charge-reorganization in the protein, *i.e.* due to the approaching negatively charge DNA electrons are repelled from the binding site in the protein (**Figure 5C, panel II**). As a result of the CISS effect, electrons with

spin parallel to their velocity move faster than those with spin aligned antiparallel to their velocity. When the DNA molecules transiently "unbind" from the protein, some of the charge is supposed to move back into the binding site, however for these electrons to move back, their spins must flip. This spin-flipping is a relatively slow process that has a lifetime of hundreds of nanoseconds, leading to a delay in the charge returning to its original state (**Figure 5C, panel III**). As a result, DNA molecules are attracted back towards the protein. This dynamic enhances their binding affinity to the protein and prevents the complete unbinding of DNA before a minimal energy conformation is reached (**Figure 5C, panel IV**).

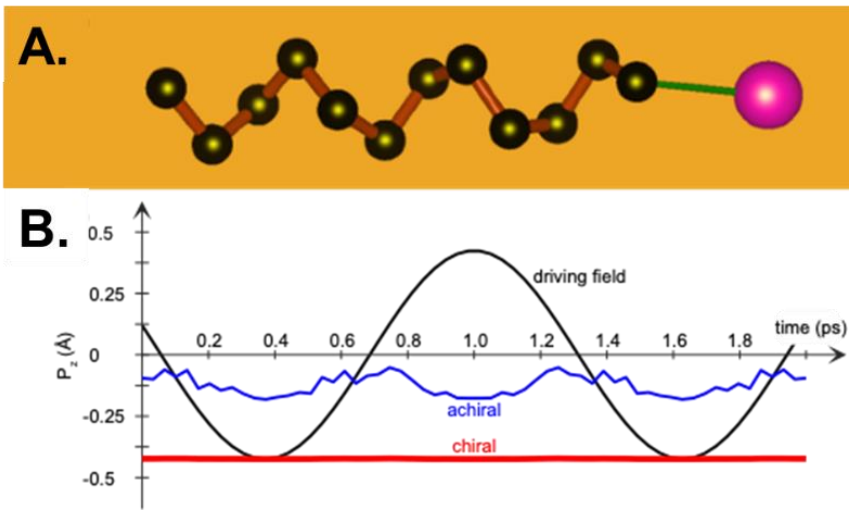

Figure 6: A. (a) Schematic of the chiral molecule (black balls, brown bonds) connected to the external charge (magenta ball, green coupling). **B**. Time-dependent variations of the electric polarization P_z for the (blue) achiral and (red) chiral molecule, under the time-dependent coupling between the molecule and external charge (black) — plotted with no reference to the vertical axis. Here, the driving frequency is $\nu_0 = 5$ THz. The sites in the molecule are elastically coupled by the nearest neighbor coupling $t_0 = 100$ meV and next-nearest neighbor coupling $\lambda_0 = 1$ meV, whereas the inelastic coupling strengths are $t_1 = t_0/10$ and $\lambda_1 = \lambda_0/10$. The molecule vibrates with the frequencies corresponding to the energies $\omega_n \in (10^{-4}, 10^{-3}, 10^{-2}, 10^{-1}, 1, 10, 10^2)$ meV, and the temperature is set to $T = 300$ K.

The proposed mechanism was tested using quantum simulations to model the dynamics of charge density within a test molecule comprising of a chain of M sites distributed in a helical or a straight chain, analogous to DNA (**Figure 6A**). Each site may hold an electron at the energy ϵ_m and is coupled to its nearest and next-nearest neighbor by both elastic (t_0, λ_0) and inelastic (t_1, λ_1) components, where the inelastic components account for nuclear vibrations that are coupled

to the electronic charge (t_1) and to the electronic spin through the spin-orbit interaction (λ_1). The chiral or achiral structures are controlled by the next-nearest neighbor interaction. The effect of the perturbing charge on the DNA is provided by an additional external electron, illustrated by the magenta ball in **Figure 6A**, where the green line between this charge and the protein signifies the (time-varying) electrostatic coupling between the entities. The details of setting up the molecule can be found in Refs. [44,45]

The simulations of the charge dynamics in the chiral and achiral chains are undertaken by varying the coupling between the external charge and the protein harmonically as $U_0 cos\hbar\nu_0 t$, where U_0 defines the maximum coupling strength, $\hbar$ is the reduced Planck's constant, ν_0 the frequency of the variations, and t is the time. The external variations acting on the molecule (driving field) is plotted in **Figure 6B** (black). The method used for the simulations of the dynamics is described in Ref. [45]

By the time-dependent variations in the local charge conditions near one of the edges of the protein, the internal charge of the protein is forced to react in response to these changes. As a measure of these variations, we calculate the electric polarization P_z of the molecule with respect to its center of mass. With this a reference, a negative (positive) polarization indicates that the average charge is pushed away from (pulled towards) the external charge. In the achiral molecule, the charge moves back and forth in response to the charge variations (blue, **Figure 6B**). This is expected since only the molecular charge is constrained, by charge conservation. However, it may transiently redistribute within the molecule and, hence, follow the time-dependence of the perturbation with a potential retardation. By contrast, in the chiral molecule, the time-dependent charge variations are negligible compared to the corresponding variations in the achiral molecule (red, **Figure 6B**). As discussed above, the underlying mechanism that prevents charge from a dynamic variation is the chiral induced spin selectivity effect, such that charge redistribution of carriers with different spins are favored in different directions. Hence, a carrier with the preferred spin that is pushed away by the external charged DNA, gives rise to a negative charge polarization. Restoration of the charge distribution as the DNA moves away from the protein, requires a spin flip of the accumulated charge. However, this spin-flip requires additional time to occur, time under which the DNA has changed its motion and is again moving towards the protein. As a result,

the internal charge dynamics of the protein is quenched and the polarization P_z, therefore, remains negative and nearly constant despite the motion of the external charge.

It is important to appreciate that interaction of protein with any binding-partner necessarily involves charge reorganization within the protein, due to the different electrochemical potentials of the protein and the binding-partner. Hence, the mechanism described above should be relevant to all association processes, in which the objects are chiral.

Conclusions

We have demonstrated that the association between model primordial polypeptides and DNA depends on electron spin. The spin effect is a result of the polarizability of the protein being spin selective due to the chiral-induced spin-selectivity (CISS) effect. The CISS effect relates homochirality (be it *L* or *D*) to the spin-dependent polarization of electrons which, in turn, influences internal charge dynamics. Therefore, there is a direct relation between homochirality and the charge dynamics within proteins that affect their function. Our study highlights an underappreciated consequence of homochirality that may have helped shape nascent biological systems. We propose that the spin selectivity enhances the binding rate between protein and substrate by elongating the relaxation time of the induced electric dipole moment in the protein. If true, spin selectivity may have promoted the emergence of homochirality. Although the proposed mechanism has yet to be confirmed by experiments, the present results provide strong evidence for the role of electron spin effects in bio-related processes, both today and in the distant past.

Materials and Methods

DNA and cloning. The synthetic gene fragments encoding P-loop prototypes were sourced from *Twist Biosciences* and inserted into a pET29(+)b expression vector using standard restriction free cloning method. Similarly, mutant prototypes were generated using standard site-directed mutagenesis via restriction-free cloning with primers obtained from *Integrated DNA Technologies* (IDT).

Protein expression and purification. P-loop prototypes have a C-terminal tag that comprises of a Trp residue for concentration determination by measuring absorbance at 280 nm (the prototypes are devoid of aromatic residues) followed by 6xHis for purification (DNA and amino acid sequences are provided in **Supplementary Tables S1 and S2**). Following purification, the yield and purity of purified proteins was assessed by SDS-PAGE (**Supplementary Figure S4**). Typically, four peak elution fractions (total 7.5 ml) were pooled together and subjected to two rounds of dialysis (two hours at room temperature plus overnight at 4 °C) in buffer containing 50 mM Tris and 100 mM NaCl (pH 8) to dialyze out the imidazole. The proteins generally precipitated during the dialysis step and required an osmolyte such as L-arginine to resolubilize the proteins. The samples were centrifuged; the protein pellet was collected and dissolved in buffer containing 50 mM Tris (pH 8), 100 mM NaCl and 1 M L-arginine (osmolyte to resolubilize the proteins). Purified prototypes, stored in this buffer at 4 °C, at 100 to 200 µM concentrations, remained soluble and active for periods of ten-fourteen days.

Peptides. Synthetic peptide constructs of N-αβα prototype harboring all *L*-amino acids (N-αβα_LcysEnd) and harboring all *L*-amino acids except for the terminal cysteine in *D*-form (N-αβα_DcysEnd) were procured from *Synpeptide*. Peptides were dissolved in 10% Acetonitrile + 90% Millipore water according to manufacturer's instructions at 2.5 mM stock concentrations. HhH peptides were synthesized inhouse (**Supplementary Figure S5**; see 'Supplementary Methods' for details). Peptides were divided into aliquots and stored at -20 ºC till further use.

Preparation of the ferromagnetic substrate. Ferromagnetic substrates were prepared as described previously [46]. An 8-nm thick Ti adhesive layer was deposited on a p-type (boron-doped), silicon (Si) ⟨100⟩±0.9° wafer. Next, a 100-nm-thick nickel (Ni) layer, that serves as ferromagnetic layer, was deposited on the adhesive coated Si wafer using an electron beam evaporator. The Ni

layer was coated with a thin gold (Au) layer of 5 nm. The evaporator chamber was kept at high vacuum ($<10^{-7}$ Torr) and ambient temperature during deposition of the metal layers. Substrates were cut into 23 × 23 mm^2 squares using diamond cutter for all microscopy experiments. The substrate pieces were cleaned by boiling in acetone for 10 mins, followed by boiling in ethanol for 10 mins and 1 min sonication in water-bath to dislodge any broken debris from the surfaces.

Drop casting/adsorbing proteins on ferromagnetic substrates. P-loop prototype proteins were diluted and dialyzed into 50 mM tris buffer, pH 8, to a final concentration of 100 μM. A ten-fold molar excess of TCEP was added to the proteins or peptides to reduce the terminal cysteines. The samples were kept at room temperature (for biologically purified proteins) or on ice (for synthetic peptides) for 3 hrs. to ensure complete reduction of all cysteine residues. The samples were filtered using BioRad *Micro Bio-Spin* P-6 columns to remove TCEP. The protein concentration was checked using a nanodrop and final concentration was adjusted to 80 μM.

The HhH peptides are dissolved in a 50 mM Tris buffer, 150 mM NaCl (pH =7.5). the final concentration of the peptides was 20 μM and it was verified using Nanodrop. Five times concentrated TCEP solution was added to avoid the formation of disulfide bonds between the peptides. Peptides were filtered using spin columns as above.

Boiled and cleaned surfaces from cleaning step described above, were dried using inert N_2 gas-gun, one at time and immediately drop-casted with 30 μl of protein sample in the center of each substrate. The substrates with drop-casted proteins were placed in a petri-dish, sealed with a parafilm and placed overnight (16 hr.) at room temperature (for biologically purified proteins) or at 4 degrees (for synthetic peptides).

Hybridization of the dsDNA for the binding kinetics experiments. The dsDNA solution was prepared by mixing the two complementary strands of ssDNA in 0.4 M phosphate buffer at pH 7.2, followed by PCR thermal incubation (60 °C for 10 min, then cooled down to 15 °C at the rate of -1 °C per min). The solution was then filtered by a Micro Bio-Spin P-30 column. The absorption of the solution was measured and diluted to final concentration of 1 μM.

Preparing substrates for microscopy experiments. Monolayer formation from overnight (16 hr.) incubation of proteins with Au-coated substrates was carried out using Polarization modulation-infrared reflection-adsorption spectroscopy (PM-IRRAS) and atomic force microscopy (see '**Supplementary Methods'**, **Supplementary Figures S7 and S8**). Overnight incubated FM-substrates were washed thrice with 1 mL of 50 mM Tris buffer (pH 8). A small scratch, using a diamond cutter was created at the center of each substrate. By locating the scratch in the microscopy experiments (discussed later) allowed us to ensure uniformity across experiments by image the center of substrates.

Microscopy measurements. We measured the binding kinetics of the ssDNA to P-loop prototypes or dsDNA to HhH peptides anchored on FM-substrates (described above) using a ZEISS Axio-Observer.Z1 inverted fluorescence widefield microscope. Prepared substrates were then placed on to a permanent 0.42 T magnet, held in place using an adhesive tape, with the North Pole facing the substrate. In parallel, a drop of 80 μl fluorescently labeled (6-FAM) ssDNA or dsDNA placed at the center of the 35 mm, glass-bottom-well, Petri dish (*MAKTEK)*, which was then transferred to the microscope stage. The assembly of the magnet with FM-substrate was then inverted onto the Petri dish containing fluorescent DNA solution.

Images were acquired using a 40× air objective lens (LD Plan-Neofluar. 40x / 0.6). Using a GFP filter, the emitted fluorescence was collected and was separated from the excitation beam by placing two dichroic beam splitters in the optical path. It was then routed to an avalanche photodiode (APD) for fluorescence imaging. Before initiating test experiments, a control experiment was carried out to focus the z-position at the surface–solution interface. This was done by locating the scratch on the FM-substrate described earlier allowed. This z-position was then fixed for all the experiments. Experiments were initiated and fluorescence intensity images were acquired using *Slidebook* software for every 30s for a duration of 15 mins. We selected the same region from each image with a size of 400 pixels × 400 pixels, located with the help of the scratch. The increase in fluorescence relative to initial fluorescence value (F/F_0) was calculated and plotted versus time. Each experiment was repeated three times to ensure the reproducibility of the results. The errors shown in the plots were calculated as the standard deviation from the mean. The entire procedure was then repeated with the South magnet pointing towards the substrate.

Macroscopic Contact Potential Difference (CPD) measurements. The CPD measurements were performed using a commercial Kelvin probe set up (Delta Phi Besocke, Jülich, Germany) confined inside a Faraday cage under atmospheric pressure. A general kelvin probe set up includes a metallic probe electrode (gold grid) which is placed near the surface of the sample to form a capacitor (**Figure 4A**). The distance between the probe electrode and the surface of the sample is periodically varied to create a frequency dependent capacitance. Now an AC voltage is generated across the gap, and this is proportional to the voltage difference between the sample and the probe electrode. Rather than measuring AC voltage directly, a DC voltage is generally applied (to nullify the response) which measures the CPD. The CPD signal is allowed to stabilize before recording.

Substrate preparation for CPD measurements. The substrates were p-doped silicon wafers Si⟨100⟩ upon which Ti/Ni/Au- 8nm/60nm/8nm with 0.3Å/sec, 0.5Å/sec, and 0.3Å/sec deposition rate at 10^{-8} Torr pressure were grown by an electron beam evaporator. After deposition, the substrates were cleaned with boiling acetone followed by boiling ethanol for 15 minutes each. Immediately after the cleaning, the substrates were dried under nitrogen flow. In parallel, the N-αβα_LcysEnd peptides were incubated with TCEP for reduction of the terminal cysteine as described in earlier section (see *Drop casting/adsorbing proteins on ferromagnetic substrates*). The peptides were purified of TCEP and drop casted on the clean-dried substrates and incubated for 16 hours at 4 ^{0}C temperature. Substrates were washed thrice with 50 mM Tris buffer (pH 8) solution, dried with inert nitrogen gas, and placed on a permanent magnet with either the North polarity facing the substrate (UP) or away from the substrate (DOWN). A drop of TC-ssDNA (same DNA that is used for microscopy experiments) was placed onto the substrates and incubated for 30 minutes. The DNA is then aspirated out with a pipette, dried under nitrogen flow and then CPD measurements were conducted.

Acknowledgements

We thank Dr. Reinat Nevo for help with microscopy experiments. RN acknowledges partial support from the US-AFSOR Grant FA9550-21-1-0418. JF acknowledges support from Vetenskapsrådet and Stiftelsen Olle Engkvist Byggmästare. NM acknowledges the support of the Israel Science Foundation (1388/22). PV acknowledges financial support from the Feinberg Graduate School, Weizmann Institute of Science.

References

1. Schreiber, G. & Fersht, A. R. Rapid, electrostatically assisted association of proteins. *Nat. Struct. Biol.* **3**, 427–431 (1996).
2. Sheinerman, F. B., Norel, R. & Honig, B. Electrostatic aspects of protein-protein interactions. *Curr. Opin. Struct. Biol.* **10**, 153–159 (2000).
3. Bauer, M. R. & Mackey, M. D. Electrostatic Complementarity as a Fast and Effective Tool to Optimize Binding and Selectivity of Protein–Ligand Complexes. *J. Med. Chem.* **62**, 3036–3050 (2019).
4. Schreiber, G., Haran, G. & Zhou, H.-X. Fundamental Aspects of Protein−Protein Association Kinetics. *Chem. Rev.* **109**, 839–860 (2009).
5. Fried, S. D., Bagchi, S. & Boxer, S. G. Extreme electric fields power catalysis in the active site of ketosteroid isomerase. *Science* **346**, 1510–1514 (2014).
6. Khoruzhii, O. *et al.* Application of a polarizable force field to calculations of relative protein-ligand binding affinities. *Proc. Natl. Acad. Sci. U. S. A.* **105**, 10378–10383 (2008).
7. Lopes, P. E. M. *et al.* Force Field for Peptides and Proteins based on the Classical Drude Oscillator. *J. Chem. Theory Comput.* **9**, 5430–5449 (2013).
8. Halgren, T. A. & Damm, W. Polarizable force fields. *Curr. Opin. Struct. Biol.* **11**, 236–242 (2001).
9. Jing, Z. *et al.* Polarizable Force Fields for Biomolecular Simulations: Recent Advances and Applications. *Annu. Rev. Biophys.* **48**, 371–394 (2019).
10. Banerjee-Ghosh, K. *et al.* Long-Range Charge Reorganization as an Allosteric Control Signal in Proteins. *J. Am. Chem. Soc.* **142**, 20456–20462 (2020).
11. Ghosh, S. *et al.* Substrates Modulate Charge-Reorganization Allosteric Effects in Protein-Protein Association. *J. Phys. Chem. Lett.* **12**, 2805–2808 (2021).

12. Naaman, R., Paltiel, Y. & Waldeck, D. H. Chiral Induced Spin Selectivity and Its Implications for Biological Functions. *Annu. Rev. Biophys.* **51**, 99–114 (2022).
13. Kumar, A. *et al.* Chirality-induced spin polarization places symmetry constraints on biomolecular interactions. *Proc. Natl. Acad. Sci. U. S. A.* **114**, 2474–2478 (2017).
14. Eck, R. V & Dayhoff, M. O. Evolution of the structure of ferredoxin based on living relics of primitive amino Acid sequences. *Science* **152**, 363–366 (1966).
15. Jayaraman, V., Toledo-Patiño, S., Noda-García, L. & Laurino, P. Mechanisms of protein evolution. *Protein Sci.* **31**, e4362 (2022).
16. Berezovsky, I. N. Towards descriptor of elementary functions for protein design. *Curr. Opin. Struct. Biol.* **58**, 159–165 (2019).
17. Vyas, P., Malitsky, S., Itkin, M. & Tawfik, D. On the Origins of Enzymes: Phosphate-Binding Polypeptides Mediate Phosphoryl Transfer to Synthesize Adenosine Triphosphate. *J. Am. Chem. Soc.* **145**, 8344–8354.
18. Söding, J. & Lupas, A. N. More than the sum of their parts: On the evolution of proteins from peptides. *BioEssays* **25**, 837–846 (2003).
19. Ma, B.-G. *et al.* Characters of very ancient proteins. *Biochem. Biophys. Res. Commun.* **366**, 607–611 (2008).
20. Alva, V., Söding, J. & Lupas, A. N. A vocabulary of ancient peptides at the origin of folded proteins. *Elife* **4**, 1–19 (2015).
21. Longo, L. M. *et al.* On the emergence of P-Loop NTPase and Rossmann enzymes from a Beta-Alpha-Beta ancestral fragment. *Elife* **9**, e64415 (2020).
22. Longo, L. M., Petrović, D., Kamerlin, S. C. L. & Tawfik, D. S. Short and simple sequences favored the emergence of N-helix phospho-ligand binding sites in the first enzymes. *Proc. Natl. Acad. Sci.* **117**, 5310 LP – 5318 (2020).
23. Saraste, M., Sibbald, P. R. & Wittinghofer, A. The P-loop — a common motif in ATP- and GTP-binding proteins. *Trends Biochem. Sci.* **15**, 430–434 (1990).
24. Lupas, A. N., Ponting, C. P. & Russell, R. B. On the evolution of protein folds: are similar motifs in different protein folds the result of convergence, insertion, or relics of an ancient peptide world? *J. Struct. Biol.* **134**, 191–203 (2001).
25. Leipe, D. D., Wolf, Y. I., Koonin, E. V. & Aravind, L. Classification and evolution of P-loop GTPases and related ATPases. *J. Mol. Biol.* **317**, 41–72 (2002).

26. Leipe, D. D., Koonin, E. V. & Aravind, L. Evolution and classification of P-loop kinases and related proteins. *J. Mol. Biol.* **333**, 781–815 (2003).

27. Walker, J. E., Saraste, M., Runswick, M. J. & Gay, N. J. Distantly related sequences in the alpha- and beta-subunits of ATP synthase, myosin, kinases and other ATP-requiring enzymes and a common nucleotide binding fold. *EMBO J.* **1**, 945–951 (1982).

28. Romero Romero, M. L. *et al.* Simple yet functional phosphate-loop proteins. *Proc. Natl. Acad. Sci.* **115**, E11943 LP-E11950 (2018).

29. Vyas, P. *et al.* Helicase-Like Functions in Phosphate Loop Containing Beta-Alpha Polypeptides. *Proc. Natl. Acad. Sci.* **118**, (2021).

30. Knowles, J. R. Enzyme-Catalyzed Phosphoryl Transfer Reactions. *Annu. Rev. Biochem.* **49**, 877–919 (1980).

31. Lassila, J. K., Zalatan, J. G. & Herschlag, D. Biological phosphoryl-transfer reactions: understanding mechanism and catalysis. *Annu. Rev. Biochem.* **80**, 669–702 (2011).

32. Gruic-Sovulj, I., Longo, L. M., Jabłońska, J. & Tawfik, D. S. The evolutionary history of the HUP domain. *Crit. Rev. Biochem. Mol. Biol.* 1–15 (2021) doi:10.1080/10409238.2021.1957764.

33. Longo, L. M., Hirai, H. & McGlynn, S. E. An evolutionary history of the CoA-binding protein Nat/Ivy. *Protein Sci.* **31**, e4463 (2022).

34. Longo, L. M. *et al.* Primordial emergence of a nucleic acid binding protein via phase separation and statistical ornithine to arginine conversion. *Proc. Natl. Acad. Sci.* **117**, 15731–15739 (2020).

35. Doherty, A. J., Serpell, L. C. & Ponting, C. P. The Helix-Hairpin-Helix DNA-Binding Motif: A Structural Basis for Non-Sequence-Specific Recognition of DNA. *Nucleic Acids Res.* **24**, 2488–2497 (1996).

36. Weil-Ktorza, O. *et al.* Functional Ambidexterity of an Ancient Nucleic Acid-Binding Domain. *bioRxiv* 2023.03.06.531422 (2023) doi:10.1101/2023.03.06.531422.

37. Seal, M. *et al.* Peptide-RNA Coacervates as a Cradle for the Evolution of Folded Domains. *J. Am. Chem. Soc.* **144**, 14150–14160 (2022).

38. Ghosh, S. *et al.* Effect of Chiral Molecules on the Electron's Spin Wavefunction at Interfaces. *J. Phys. Chem. Lett.* **11**, 1550–1557 (2020).

39. Levitt, M. & Lifson, S. Refinement of protein conformations using a macromolecular

energy minimization procedure. *J. Mol. Biol.* **46**, 269–279 (1969).

40. Polo, S. E. & Jackson, S. P. Dynamics of DNA damage response proteins at DNA breaks: a focus on protein modifications. *Genes Dev.* **25**, 409–433 (2011).
41. Chen, T.-Y., Cheng, Y.-S., Huang, P.-S. & Chen, P. Facilitated Unbinding via Multivalency-Enabled Ternary Complexes: New Paradigm for Protein–DNA Interactions. *Acc. Chem. Res.* **51**, 860–868 (2018).
42. Safieh, J. *et al.* DNA dynamics dictates p53 functional outcome. *bioRxiv* 2021.09.18.460898 (2021) doi:10.1101/2021.09.18.460898.
43. Khatua, S. & Taraphder, S. In the footsteps of an inhibitor unbinding from the active site of human carbonic anhydrase II. *J. Biomol. Struct. Dyn.* **41**, 3187–3204 (2023).
44. Fransson, J. Vibrational origin of exchange splitting and ' 'chiral-induced spin selectivity. *Phys. Rev. B* **102**, 235416 (2020).
45. Fransson, J. Charge and Spin Dynamics and Enantioselectivity in Chiral Molecules. *J. Phys. Chem. Lett.* **13**, 808–814 (2022).
46. Santra, K., Lu, Y., Waldeck, D. H. & Naaman, R. Spin Selectivity Damage Dependence of Adsorption of dsDNA on Ferromagnets. *J. Phys. Chem. B* **127**, 2344–2350 (2023).